Electromechanical properties of polyanilines prepared by two different approaches and their applicability in force measurements

C. Della Pina [a], E. Zappa [b], G. Busca [b], A. Sironi [a], E. Falletta [a,*]

[a] *Dipartimento di Chimica, Università degli Studi di Milano, ISTM-CNR, via C. Golgi, 19, 20133 Milano, Italy*
[b] *Dipartimento di Meccanica, Politecnico di Milano, via La Masa, 1, 20158 Milano, Italy*

Received 28 February 2014
Received in revised form 29 April 2014
Accepted 30 April 2014
Available online 17 May 2014

1. Introduction

The use of stress/strain sensors is widespread in many fields of modern life and thanks to their efficiency and sensitivity digital technologies have benefited. Owing to their application in force, pressure and strain measurements, they can be successfully employed in industry, for example as an integral part of air conditioning, heating and ventilation systems, general instrumentation, petrochemical plants or in the automotive industrial segment, this latter being the most relevant one since pressure sensors are essential in tire pressure monitoring systems, engine management and automatic transmission. Moreover, they are useful for general and consumer applications in household appliances, altimeters and scuba gears or for medical implementations, such as aerosol drug delivery, infusion pumps, intracranial measurement, low-cost disposable devices for catheters employed in surgical operations, just to mention a few [1–3].

So it is not surprising that reliable, high performance and low cost sensors are more and more valued and required, relying also on the opportunities of miniaturization offered by micro- and nano-technologies. It is esteemed that the pressure sensors market, which accounted for $5.11 billion in 2011, could reach $7.34 billion in 2017 [4]. Owing to the growing interest in this sector, in recent years organic polymers have been investigated as active materials in pressure sensors [5–9].

Among them, polyaniline (PANI, Fig. 1) and polypyrrole (PPY) are the most intriguing and studied [10–15]. The fascination for PAN is due, on the one hand, to its ease of synthesis and high environmental stability and, on the other hand, to its versatile features strictly related to the different chemical–physical characteristics of the three existing forms, classified upon the chain oxidation grade, i.e. the amount of benzenoid and quinoid units.

Only the half-oxidized and half-protonated form, emeraldine salt (ES), shows electroconductive properties and for this reason it has received a huge attention.

According to the growing environmental constraints invoking to substitute the traditional polluting synthetic methods with eco-friendly protocols, recently we addressed our efforts to find novel "green" approaches for the synthesis of conducting organic polymers, in particular polypyrrole and polyaniline [16–18].

Recently, many studies have been carried out to clarify the dependence of conductivity on applied pressure only for polyaniline prepared by traditional methods [19–24].

Herein, we report a comparison on the variation of resistance as a function of the applied load (or compression) between pellets of polyanilines prepared following two different approaches, a traditional [25] and a green one [26], identified from now on as PANI1 and PANI2 respectively.

In particular, the present paper will be focused on the investigation of the electromechanical properties of PANI1 and PANI2, in

* Corresponding author. Tel.: +39 0250314410.
E-mail address: ermelinda.falletta@unimi.it (E. Falletta).

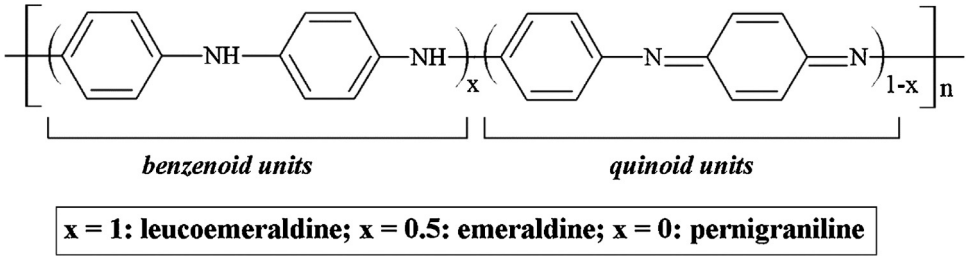

Fig. 1. Polyaniline structure.

order to clarify and encourage the exploitation of the green material in the field of pressure and force sensing.

2. Materials and methods

2.1. Reagents and instruments

N-(4-Aminophenyl)aniline (aniline dimer, AD) (Sigma Aldrich, ≥98%), aniline (Aldrich, 99%), $(NH_4)_2S_2O_8$ (Sigma Aldrich, ≥98%), H_2O_2 (Fluka, 30%), HCl (Carlo Erba, 37%), iron trichloride hexahydrate (Fluka ≥99%), ammonia solution (ProLabo 28%), H_2SO_4 (Sigma Aldrich, 98%), acetone (Sigma Aldrich, ≥99.8%), *N*,*N*-dimethylformamide (Sigma Aldrich, 99.8%), KBr (Sigma Aldrich, ≥99%) were used as received without further purification.

FT-IR spectra of KBr dispersed samples were recorded on a JASCO FT/IR-410 spectrophotometer in the 500–4000 cm^{-1} range. The UV–vis spectra were recorded on a Hewlett Packard 8453 spectrophotometer using *N*,*N*-dimethylformamide as solvent. XRD analyses were performed using a Rigaku D IIIMAX horizontal-scan powder diffractometer with Cu Kα radiation. The morphological characterization of the products was performed by scanning electron microscopy (SEM; LEO 1430 microscope). PANI pellets having diameter of 13 mm and thickness of 1 mm were prepared by pressing 200 mg of each material for 30 min at 100 kN using an Atlas Manual Hydraulic Press. Uniaxial compression tests were carried out by means of a MTS alliance RT/100 universal mechanical test machine. Resistance measurements were collected by a 5300 ICE multimeter.

2.2. Synthesis of polyaniline

Polyaniline was synthesized according to two different protocols: a traditional method based on the oxidative polymerization of aniline by the use of a stoichiometric oxidant (PANI1) [25] and a green route that employs *N*-(4-aminophenyl)aniline as the reagent and H_2O_2 as the oxidizing agent in the presence of Fe^{3+} as the catalyst (PANI2) [26].

2.3. Synthesis of PANI1

5 g of aniline (54 mmol) were dissolved in 40 mL of 5 M HCl and cooled at 4 °C. Then, 80 mL of 1.2 M $(NH_4)_2S_2O_8$ (APS) were added dropwise (APS/aniline = 1.8, molar ratio). After stirring for 6 h a green product was collected by filtration on a Büchner funnel, washed several times with water and acetone (to remove organic soluble oligomers) and dried under air. The green powder was spectroscopically characterized and identified as emeraldine salt (ES1). 2 g of ES1 were stirred in 20 mL of 1 M NH_4OH. After 24 h the mixture was filtered, a solid product (emeraldine base, EB1) was collected and washed several times with water until the mother liquor became neutral and air dried. 1 g of EB1 was reprotonated (redoped) with 18 mL of 0.3 M H_2SO_4 (aniline/H_2SO_4 = 2, molar ratio) thus obtaining PANI1.

2.4. Synthesis of PANI2

2 g of *N*-(4-aminophenyl)aniline (aniline dimer, AD) were dissolved in 50 mL of 0.2 M HCl (AD/HCl = 1, molar ratio) at room temperature. Then, 6.8 mL of H_2O_2 30% (H_2O_2/AD = 5, molar ratio) were added into the grey mixture, followed by 2.95 mg of $FeCl_3{\cdot}6H_2O$ (AD/Fe^{3+} = 1000, molar ratio). After 24 h an insoluble green product was collected by filtration, washed several times with water and acetone and air dried. The product, spectroscopically characterized and identified as emeraldine salt (ES2), was treated as reported above (Section 2.3) to obtain first EB2 and then PANI2.

2.5. Electromechanical characterization

The experimental setup described in this section aims at testing the performances of each of the two PANI types in order to analyze the response at repeat loading and unloading cycles in quasi-steady conditions.

The measurements of electrical conductivity as a function of the applied force were carried out at room temperature on pellets of PANI1 and PANI2.

All uniaxial compression tests were carried out with a MTS alliance RT/100 universal mechanical test machine that allows maximum loads of 100 kN both for tensile and compression with a maximum velocity of 508 mm/min. The tests can be controlled in force or displacements by the MTS Testworks 4 control software, which allows customizable loads or displacement laws. In this work, the MTS system was operated in force control. The axial loads were measured by a load cell MTS 4501058, with ±100 kN measurement range and 0.1 V/kN sensitivity, whereas the axial displacements were measured by a deflectometer MTS model 632.06H-30 with ±12.5 mm measurement range.

In order to perform the tests, a support for PANI was designed, as shown in Fig. 2. The sensor support had to ensure a twofold function: distributing the loading on the PANI surface in order to guarantee a proper sensor working and at the same time allowing the electric connection between the sensor surface and the measuring device used to estimate the electric resistance. For this purpose, PANI was sandwiched between two copper electrodes connected to a multimeter, whereas the deflectometer allowed to measure the displacement of the steel discs, rigidly connected to the PANI samples. The sensor and the copper plates were finally electrically isolated with respect to the loading machine by means of a thin non-conductive film.

For each PANI sample three loading/unloading cycles from 0 kN to a maximum of 100 kN with a loading step of 10 kN were performed by the use of a universal mechanical test machine. For each loading step the force was maintained constant in order to allow the PANI stabilization at the new pressure level, whereas crosshead speed from a step to the next one was fixed to 0.07 mm/min. The first cycle was performed only on the support components (Fig. 2) in the absence of any PANI pellet, in order to estimate the deformation

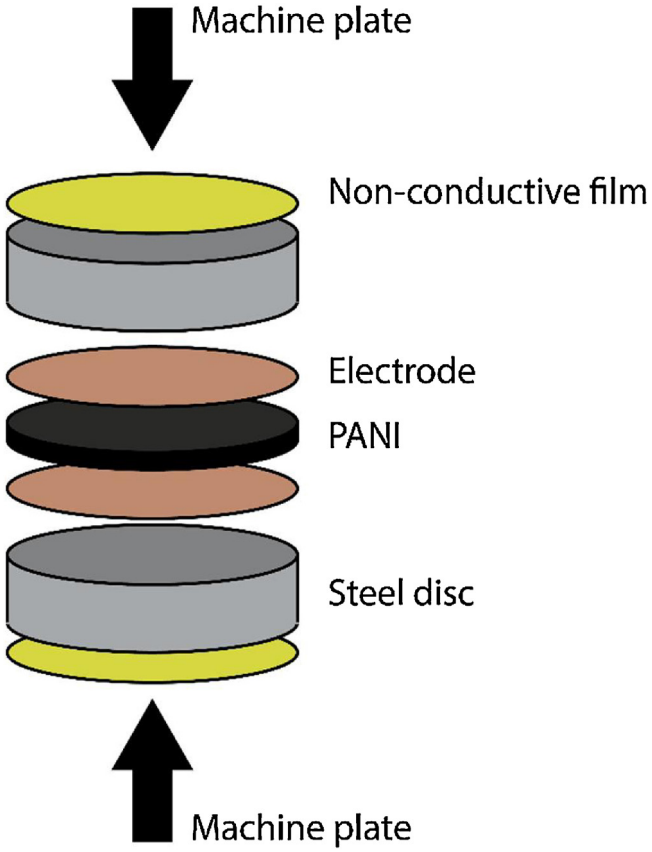

Fig. 2. PANI support for compression tests.

of these parts under the same loading conditions of the full PANIs tests. Then, the first loading/unloading cycle, done with a maximum force comparable to the one applied for the creation of the PANI pellets, was necessary to geometrically stabilize the samples and put them in complete contact with the loading plates; whereas the other two were done in order to verify the measurement repeatability. Since each sample was mounted in a sandwich, provided with electrical connections and finally isolated with respect to the loading machine, the stabilization cycle was also fundamental to allow that the overall system reached a stable condition. The electrical conductivities were estimated indirectly from resistivity measurements.

Table 1
Testing conditions.

Cycle 0	Zero setting (without PANI)	0–100 kN step 10 kN
Cycle 1	PANI stabilization	0–100 kN step 10 kN
Cycle 2	1st stabilized cycle	0–100 kN step 10 kN
Cycle 3	2nd stabilized cycle	0–100 kN step 10 kN

Table 1 summarizes the testing conditions.

3. Results and discussion

3.1. Structural characterization

PANI1 and PANI2 were characterized by FT-IR and UV–vis spectroscopies and the results are reported in Fig. 3A and B.

Both materials show the characteristic bands of polyaniline in the form of conductive emeraldine salt. In particular, concerning FT-IR spectra (Fig. 3A) the band at 1570 cm^{-1} can be assigned to the C=C stretching of the quinoid rings (N=Q=N), whereas the band at 1498 cm^{-1} corresponds to the C=C stretching vibration mode of the benzenoid rings (N–B–N). C–N and C=N stretching modes are responsible of the bands at 1311 cm^{-1} and 1246 cm^{-1} respectively, whereas those at 1027 cm^{-1} and 889 cm^{-1} are strictly related to the in-plane and out-of-plane bending of C–N. The bands at 754 cm^{-1} and 692 cm^{-1} are assigned to the deformation vibration modes of the aromatic rings, while the band at 573 cm^{-1} is typical of a 1,4 di-substituted benzene [27].

The UV–vis spectra (Fig. 3B) of both products display two characteristic bands at 311 and 603 nm. The first one is related to the π–π^* transition of the benzenoid rings, whereas the other one at 603 nm is due to the transition from a localized benzenoid highest occupied molecular orbital to a quinoid lowest unoccupied molecular orbital, that is a benzenoid to quinoid excitonic transition [28].

Even though PANI1 and PANI2 show very similar molecular structures, X-ray powder diffraction (XRPD) technique emphasizes important differences in the crystalline content of PANI1 and PANI2 (Fig. 4).

In particular, PANI1 results to be partly crystalline, whereas PANI2 is essentially an amorphous material. Both XRPD patterns exhibit a broad peak at $2\theta = 20°$, typical of amorphous PANI, but in the case of PANI1 other three weak crystalline peaks appear at $2\theta = 15°$, 20° and 26°. According to the literature [24,29–31], the crystallinity degree of polyaniline is related to several factors, such

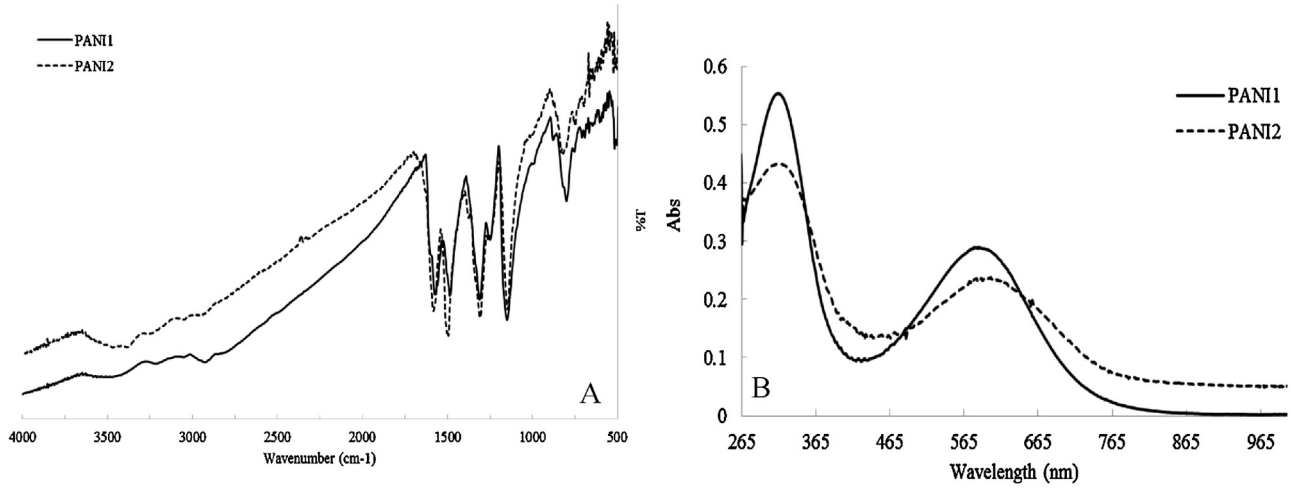

Fig. 3. FT-IR (A) and UV–vis (B) spectra of PANI1 and PANI2.

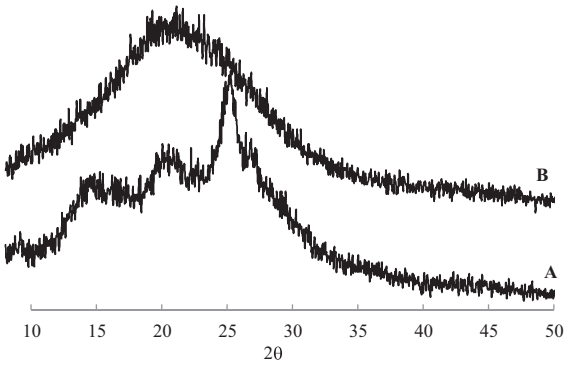

Fig. 4. XRPD patterns of PANI1 (A) and PANI2 (B).

as the reaction conditions, the kind and amount of acid used as doping agent and the molecular weight. More in detail, the crystallinity degree of PANI increases as the dopant/N ratio [29] and the molecular weight [30] increase. However, it is not directly related to the conductivity of the polymer [31]. Herein, PANI1 and PANI2 were prepared by two approaches that differ for many parameters, such as reaction temperature, reaction time, kind of oxidant and reactants, that might justify the observed difference in crystallinity degree.

Although each of these parameters can affect the crystallinity of the polymer, a deepened investigation has not yet been performed because out of the scope of this paper. However, previous results showed that PANI2 is characterized by higher solubility in common organic solvents [26] and lower conductivity values (see [20] and Table 2) than PANI1 [24], that could suggest its lower molecular weight.

Finally, as shown in Fig. 5, both PANI1 and PANI2 exhibit an irregular granular morphology, demonstrating that the latter does not affect the polymers performance.

3.2. Mechanical response

The mechanical response of both PANI1 and PANI2 was evaluated in force–compression tests for three loading/unloading cycles (Fig. 6A and B).

In order to estimate the compression of PANI1 and PANI2 avoiding the contribution of the support deformation, each force–displacement cycle, shown in Fig. 6, was obtained by subtracting the force–displacement cycle related to the support without PANI under the same loading conditions.

As it is possible to observe, loading/unloading curves do not coincide during the successive cycles and mechanical hysteresis, evident for both materials during the first loading cycle, decreases thus suggesting a mechanical stabilization of the materials.

This behaviour could be attributed to the high brittleness of these materials that does not allow the recovery of the initial microstructure after the first loading step.

Two different regimes are noticed for PANI1 for compression smaller and larger than ~0.04 mm.

In the first zone (compression < 0.04 mm) the overall nonlinear behaviour could be due to the presence of voids among the polymeric chains, that might be reduced by increasing the applied load leading to a nearly linear trend in the second region (compression > 0.04 mm). On the contrary, the more linear and almost hysteresis-free behaviour of PANI2 for all the range could suggest a different chain network leading to a more compact structure.

Negative values of compression at very low force values are likely due to the crushing of the copper electrodes (shown in Fig. 2) during the stabilization cycle.

Table 2
Maximum values of conductivity and resistance for each cycle for PANI1 and PANI2.

Sample	$\sigma_{cycle\ 1}$ (S/cm)	$\sigma_{cycle\ 2}$ (S/cm)	$\sigma_{cycle\ 3}$ (S/cm)	R (Ω)
PANI1	9.44×10^{-3}	6.83×10^{-3}	6.92×10^{-3}	436
PANI2	4.86×10^{-5}	4.90×10^{-5}	4.93×10^{-5}	48,600

3.3. Electrical conductivity

The resistance value of a resistor is given by Eq. (1):

$$R = \rho \frac{\ell}{A} \tag{1}$$

where R is the electrical resistance (Ohm), ρ is the bulk resistivity (Ohm cm), ℓ is the length of the material (cm) and A is the cross-sectional area of the specimen (cm^2) that was maintained constant during the tests.

As a consequence, conductivity σ (S/cm) can be obtained as follows:

$$\sigma = \left(\frac{1}{R}\right) \cdot \left(\frac{\ell}{A}\right) \tag{2}$$

Concerning the conductivity variation of PANI pellets with the pressure, even though several papers have been published [32,21,22,33], the differences in the doping agent used, investigated range of force/pressure and employed instrumental setup strongly affect the results thus making difficult an accurate comparison of the literature data. For example, Zhang reached a value of conductivity of 7.56 S/cm under a pressure of about 70 MPa for PANI doped with *p*-toluene sulfonic acid [22], whereas Varma and Jayalekshmi observed a conductivity of 3.11 S/cm under a maximum pressure of 30 MPa for PANI doped with naphthalene-2-sulphonic acid [33] and Bao et al. demonstrated that the resistance of PANI doped with different acids passes from 101 to 106 Ω under different pressure loadings up to 22 GPa [32].

In Fig. 7 the variation of conductivity with applied force for both polymers, PANI1 and PANI2, are reported.

As observed for the force–compression curves reported in Fig. 6, also the trends of conductivity as a function of force do not coincide for PANI1 during loading/unloading cycles, owing to its mechanical instability. In fact, the higher crystallinity degree of PANI1 (Fig. 4A) implies a higher brittleness of the polymeric chains that can reduce the mechanical properties of the polymer. However, after the first loading cycle the pellet displays a more regular behaviour with smaller hysteresis and more reproducible trends.

On the contrary, owing to its amorphous characteristics (Fig. 4B) PANI2 exhibits a more regular and reproducible behaviour and smaller hysteresis for all loading/unloading cycles.

Considering the three loading/unloading cycles the maximum values of conductivity at 100 kN and the maximum values of resistance at 0 kN for PANI1 and PANI2 are reported in Table 2.

Accordingly, the conductivity values of PANI2 are more constant and much lower than those of PANI1. As mentioned above (Section 3.1), the difference in conductivity can be related to the difference in crystallinity degree but also to the molecular weight.

The results reported in Table 2 suggest that the higher crystallinity degree of PANI1 guarantees high values of conductivity but at the same time worse mechanical properties, as shown by the stress–compression curves (Fig. 6A). On the contrary, the low degree of PANI2 crystallinity implies lower values of conductivity but better mechanical features (Fig. 6B). Moreover, the higher electrical resistance of PANI2 allows to reduce the self-heating due to Joule effect (because it is possible to use a lower excitation current to obtain the same voltage output) and to neglect the

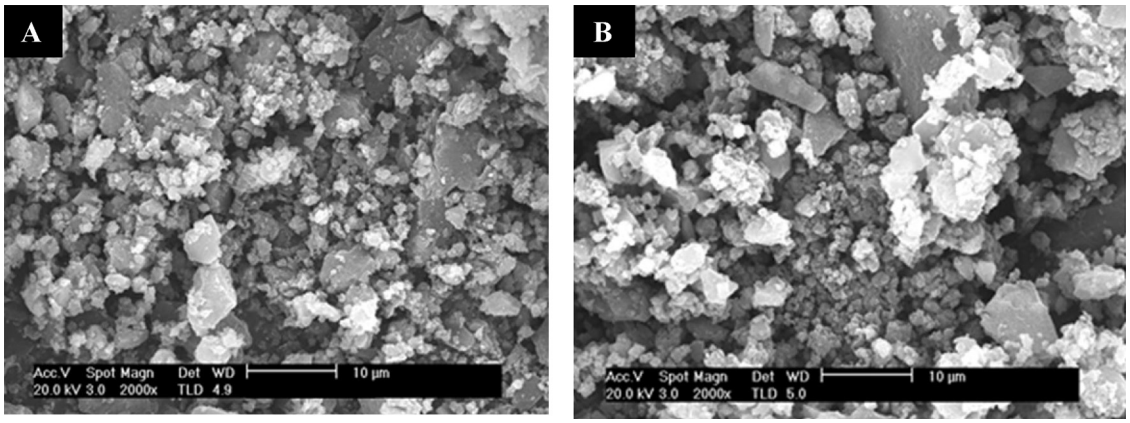

Fig. 5. SEM images of PANI1 (A) and PANI2 (B).

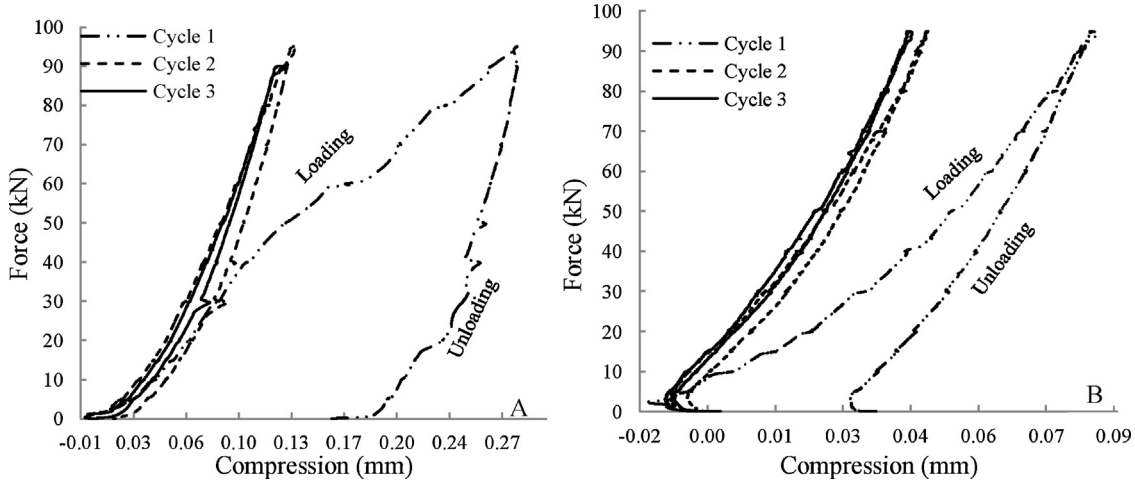

Fig. 6. Force vs compression curves under loading/unloading cycles for (A) PANI1 and (B) PANI2.

resistance of the connecting cables in most of the practical applications. Thanks to these characteristics and the above-mentioned higher mechanical properties, PANI2 is more suitable than PANI1 for sensors development.

If compared to the results from the literature reported above [32,21,22,33], our conductivity data result to be too low. This apparent incongruity is actually related to the PANI conductivity dependence on the kind of acid employed for the doping process. The dopant, in fact, can be organic or inorganic, as well as containing monovalent or multivalent ions. Moreover, the pH value of the medium wherein PANI is protonated represents a further parameter affecting the final conductivity. In this regard, the conductivity results reported in Table 2 are of the same magnitude as those obtained from Gupta et al. (from 4.2×10^{-9} to 2.0×10^{-2} S/cm) [34].

3.4. Electromechanical performances under uniaxial compression

It can be seen from Fig. 8 that the fractional change in the electrical resistance ($\Delta R/R_0$) decreases proportionally and reversibly during uniaxial compression (loading) and increases during expansion process (unloading) for both materials.

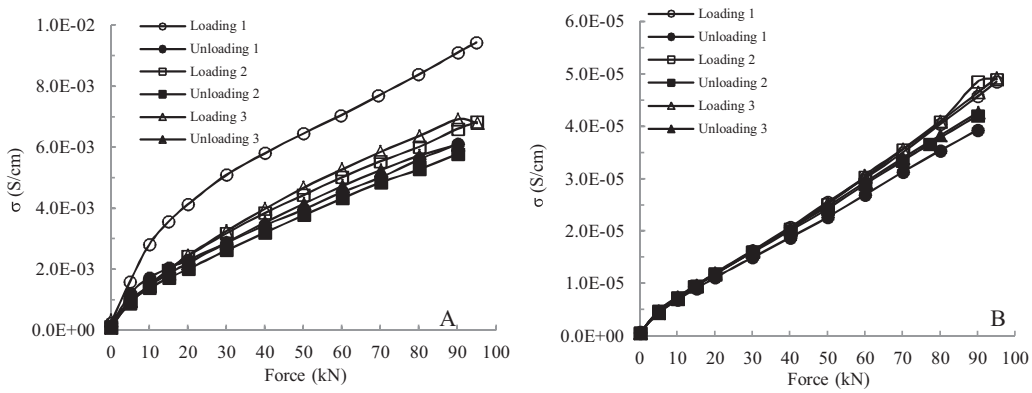

Fig. 7. Conductivity (S/cm) as a function of force (kN) for (A) PANI1 and (B) PANI2.

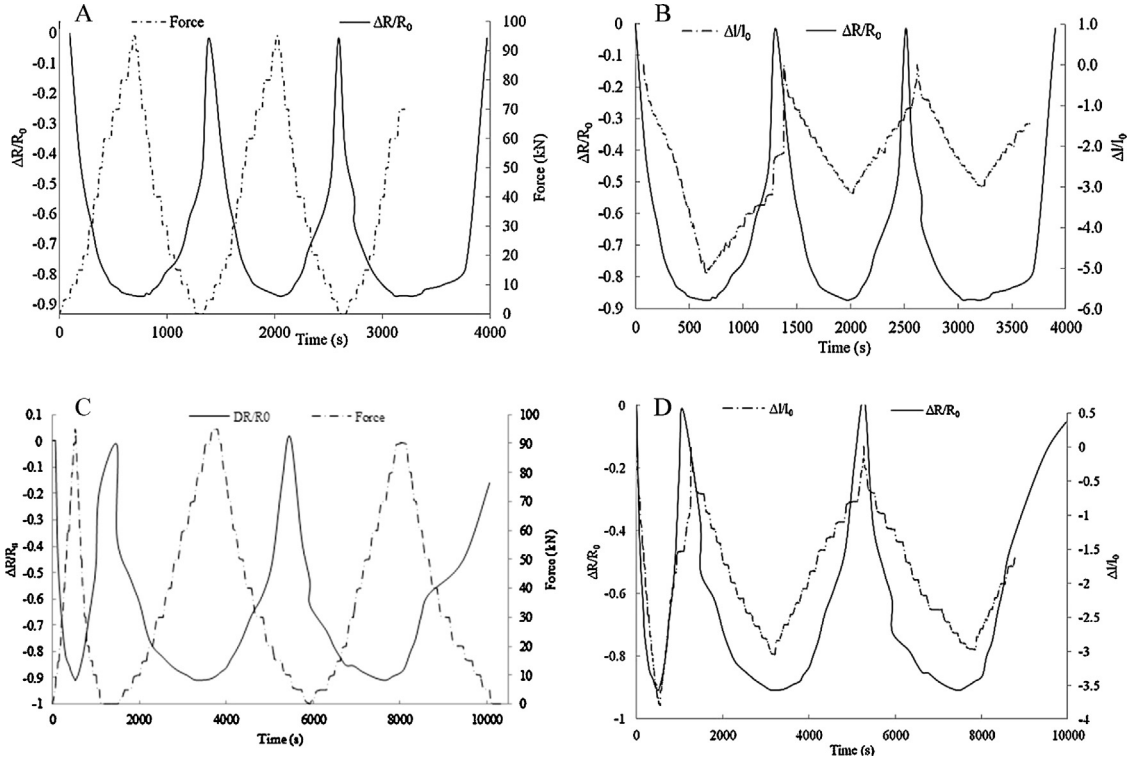

Fig. 8. Resistance variation ($\Delta R/R_0$) with deformation ($\Delta l/l_0$) for (A) PANI1 and (C) PANI2 and with applied force for (B) PANI1 and (D) PANI2.

Electrical resistance changes up to about 90% for both PANI1 and PANI2 when the compressive stress is in the range of 0–100 kN. The relationship between change in resistance and deformation is expressed in terms of gauge factor equation (3):

$$\mathrm{GF} = \frac{\Delta R/R_0}{\Delta l/l_0} \tag{3}$$

where R_0 is the steady-state electrical resistance of the material without deformation (l_0) and ΔR is the resistance variation caused by the change in length (Δl) [35]. This quantifies the magnitude of the piezoresistivity effect.

In Fig. 9 the fractional change in electrical resistance ($\Delta R/R_0$) is plotted as a function of the deformation $\Delta l/l_0$, together with the linear regression line for both PANI1 and PANI2.

The slope of the linear fit, according to Eq. (3) (obtained with a *R*-square higher than 0.90), corresponds to the GF values of the samples.

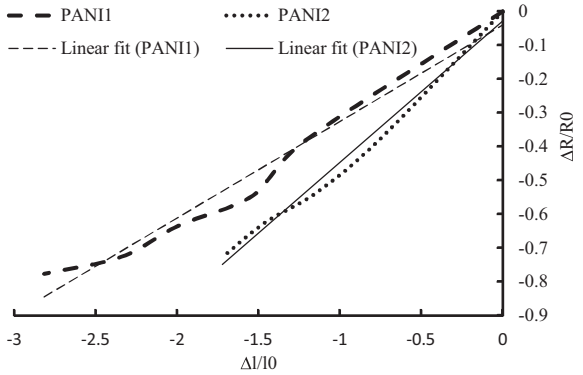

Fig. 9. Fractional change in electrical resistance as a function of the deformation for PANI1 and PANI2.

For PANI1 and PANI2 GFs resulted to be 0.29 and 0.42 respectively, typical values of commercial stress/strain sensors (GF of 0.1–2), whose change in resistance is only due to geometric effects [36].

However, starting from Eq. (1), it is possible to affirm that the resistance variation of a material is related to two parameters: the change of resistivity (ρ), that is an intrinsic property of each material, and the geometrical variation ℓ/A. As reported in the literature [37], the former parameter has a more important effect on the gauge factor than the latter one. Moreover, it is known that the conduction mechanism of polyaniline is the sum of two different contributions: the ability of charge carriers to move along the backbone (*intra*-chain mechanism) and their ability to hop between chains (*inter*-chain mechanism) [38]. This second contribution becomes particularly important during the stress/strain processes, influencing the ρ value of the polymer and consequently its resistance.

Therefore, the low GF values observed for both PANI1 and PANI2 suggest two considerations: on the one hand we could affirm that when the polymer is employed in the form of pellet the contribution of the geometrical deformation on the resistance change is higher than that of the resistivity variation, because the effect of the *inter*-chain displacement is suppressed by the random orientation of chains in the pellet; on the other hand the *inter*-chain displacement could be reduced by the use of a small doping agent (H_2SO_4, as in this case).

Hence, in order to increase the first parameter of Eq. (1) (resistivity change) and as a consequence the GF values of polyaniline, the polymer should be employed in nanosized scale to reduce as much as possible the contribution of geometrical deformation and, at the same time, a big dopant (e.g. organic acids) should be used to emphasize the *inter*-chain displacement.

4. Conclusions

It was demonstrated that both the mechanical and electrical behaviour of polyanilines prepared by two different approaches is strictly related to their degree of crystallinity. In particular, the semi-crystallinity of PANI1 guarantees high values of conductivity but, at the same time, high brittleness of the material thus compromising its mechanical performances. On the contrary, the amorphous PANI2 exhibits values of conductivity two order of magnitude lower than PANI1 but higher mechanical performances thus making it more suitable for pressure and force measurements. Furthermore, PANI2 shows a more linear electromechanical response than PANI1, that is crucial for sensor applications. Finally, the similar low GF values of both PANI1 and PANI2 could be related to the use of PANI in pellet form but also to the small dimensions of the doping agent (H_2SO_4). In fact, both these factors can reduce the contribution of the *inter*-chain conduction mechanism and emphasize the geometrical contribution to the resistance change. The results obtained for PANI2 are particularly important because they can open the way to a new generation of green polyanilines in the field of force/pressure sensors.

References

[1] K.B. Mundy, J.X. Yu, U.S. Pat. Appl. Publ., US 20100082162 A1 20100401 (2010).
[2] M.R.A. Hassan, N. Tamchek, A.F. Abas, R.M. Johar, F.R. Mahamd Adikan, Dual-phase sensing for early detection of prepreg structural failures via etched cladding Bragg grating, Sens. Actuators A: Phys. 171 (2) (2011) 126–130.
[3] K. Milburn, U.S. Pat. Appl. Publ., US 20120265395 A1 20121018, (2012).
[4] http://www.marketsandmarkets.com/Market-Reports/pressure-sensor-market-871.html
[5] E. Klimiec, W. Zaraska, J. Piekarski, B. Jasiewicz, PVDF sensors – research on foot pressure distribution in dynamic conditions, Adv. Sci. Technol. 79 (2013) 94–99.
[6] X. Zheng, C.-Y. Han, A micro pressure sensor based on SU-8 polymer, Appl. Mech. Mater. 220–223 (2012) 1902–1905.
[7] B.C.-K. Tee, C. Wang, R. Allen, Z. Bao, An electrically and mechanically self-healing composite with pressure- and flexion-sensitive properties for electronic skin applications, Nat. Nanotechnol. 7 (2012) 825–832.
[8] C.P. Fernandes, P.O.J. Glantz, S.A. Svensson, A. Bergmark, A novel sensor for bite force determinations, Dental Mater. 19 (2003) 118–126.
[9] G.S. Gupta, P. Barlow, S. David, Instrumentation and Measurement Technology Conference (I2MTC), 2011, pp. 1–5.
[10] X.-G. Li, Q.-F. Lu, M.-R. Huang, Self-stabilized nanoparticles of intrinsically conducting copolymers from 5-sulfonic-2-anisidine, Small 4 (2008) 1201–1209.
[11] X.-G. Li, A. Li, M.-R. Huang, Facile high-yield synthesis of polyaniline nanosticks with intrinsic stability and electrical conductivity, Chem. – Euro. J. 14 (2008) 10309–10317.
[12] X.-G. Li, H. Feng, M.-R. Huang, G.-L. Gu, M.G. Moloney, Ultrasensitive Pb(II) potentiometric sensor based on copolyaniline nanoparticles in a plasticizer-free membrane with a long lifetime, Anal. Chem. 84 (2012) 134–140.
[13] X.-G. Li, Z.-Z. Hou, M.-R. Huang, M.G. Moloney, Efficient synthesis of intrinsically conducting polypyrrole nanoparticles containing hydroxy sulfoaniline as key self-stabilized units, J. Phys. Chem. C 113 (2009) 21586–21595.
[14] X.-G. Li, A. Li, M.-R. Huang, Y. Liao, Y.-G. Lu, Efficient and scalable synthesis of pure polypyrrole nanoparticles applicable for advanced nanocomposites and carbon nanoparticles, J. Phys. Chem. C 114 (2010) 19244–19255.
[15] X.G. Li, Simple synthesis of intrinsically conducting polyaniline by a chemically oxidative polymerization, E-Polymers (2007) E-002.
[16] C. Della Pina, E. Falletta, M. Lo Faro, M. Pasta, M. Rossi, Gold-catalysed synthesis of polypyrrole, Gold Bull. 42 (2009) 27–33.
[17] Z. Chen, C. Della Pina, E. Falletta, M. Lo Faro, M. Pasta, M. Rossi, N. Santo, Facile synthesis of polyaniline using gold catalyst, J. Catal. 259 (2008) 1–4.
[18] Z. Chen, C. Della Pina, E. Falletta, M. Rossi, A green route to conducting polyaniline by copper catalysis, J. Catal. 367 (2009) 93–96.
[19] X.-R. Zeng, K.-C. Gong, K.-N. Weng, W.-S. Xiao, W.-H. Gan, T.-M. Ko, Effects of ultra-high pressures (>3.6 GPa) on the electrical resistance of polyaniline by in situ FT-IR studies, Chem. Phys. Lett. 280 (1997) 469–474.
[20] H.G. Kiess, Conjugated Conducting Polymers, Springer, New York, 1992, pp. 140–145.
[21] Z.X. Bao, C.X. Liu, P.K. Kahol, N.J. Pinto, Pressure dependence of the resistance in polyaniline and its derivatives at room temperature, Syn. Metals 106 (1999) 107–110.
[22] D. Zhang, On the conductivity measurement of polyaniline pellets, Polym. Test. 26 (2007) 9–13.
[23] F.G. de Souza Jr., T.K. Anzai, P.A. Melo Jr., B.G. Soares, M. Nele, J.C. Pinto, Influence of reaction media on pressure sensitivity of polyanilines doped with DBSA, J. Appl. Polym. Sci. 107 (2008) 2404–2413.
[24] M. Pyo, J.-H. Hwang, Conductivity changes of dodecylbezensulfonic acid-doped polyaniline during pressure loading/unloading, Syn. Metals 159 (2009) 700–704.

[25] J.C. Chang, A.G. MacDiarmid, 'Polyaniline': protonic acid doping of the emeraldine form to the metallic regime, Syn. Metals 13 (1986) 193–205.
[26] P. Frontera, C. Busacca, S. Trocino, P. Antonucci, M. Lo Faro, E. Falletta, C. Della Pina, M. Rossi, Electrospinning of polyaniline: effect of different raw sources, J. Nanosci. Nanotechnol. 13 (2013) 4744–4751.
[27] X. Feng, C. Mao, G. Yang, W. Hou, J. Zhu, Polyaniline/Au composite hollow spheres: synthesis, characterization, and application to the detection of dopamine, Langmuir 22 (2006) 4384–4389.
[28] K. Mallick, M.J. Witcomb, A. Dinsmore, M.S. Scurrell, Polymerization of aniline by cupric sulfate: a facile synthetic route for producing polyaniline, J. Polym. Res. 13 (2006) 397–401.
[29] J.P. Pouget, M.E. Jdzefowiczt, A.J. Epstein, X. Tang, A.G. MacDiarmid, X-ray structure of polyaniline, Macromolecules 24 (1991) 779–789.
[30] K.S. Ryu, S.H. Chang, S.-G. Kang, E.J. Oh, C.H. Yo, Physicochemical and electrical characterization of polyaniline induced by crosslinking, stretching, and doping, Bull. Korean Chem. Soc. 20 (1999) 333–336.
[31] H.K. Chaudhari, D.S. Kelkar, X-ray diffraction study of doped polyaniline, J. Appl. Polym. Sci. 62 (1996) 15–18.
[32] Z.-X. Bao, C.X. Liu, N.J. Pinto, Electrical conductivity of polyaniline as a function of pressure using a diamond anvil cell, Syn. Metals 87 (1997) 147–150.
[33] S.J. Varma, S. Jayalekshmi, On the prospects of polyaniline and polyaniline/MWNT composites for possible pressure sensing applications, J. Appl. Polym. Sci. 117 (2010) 138–142.
[34] S.K. Gupta, V. Luthra, R. Singh, Electrical transport and EPR investigations: a comparative study for d.c. conduction mechanism in monovalent and multivalent ions doped polyaniline, Bull. Mater. Sci. 35 (5) (2012) 787–794.
[35] M. Knite, V. Teteris, A. Kiploka, J. Kaupuzs, Polyisoprene–carbon black nanocomposites as tensile strain and pressure sensor materials, Sens. Actuators A: Phys. 110 (2004) 142–149.
[36] E. Defaÿ, C. Millon, C. Malhaire, D. Barbier, PZT thin films integration for the realisation of a high sensitivity pressure microsensor based on a vibrating membrane, Sens. Actuators A: Phys. 99 (2002) 64–67.
[37] J.G. Rocha, A.J. Paleo, F.W.J. van Hattum, S. Lanceros-Mendez, Polypropylene–carbon nanofiber composites as strain-gauge sensor, IEEE Sens. J. 13 (7) (2013) 2603–2609.
[38] W.W. Focke, G.E. Wnek, Y. Wei, Influence of oxidation state, pH, and counterion on the conductivity of polyaniline, J. Phys. Chem. 91–22 (1987) 5813–5818.